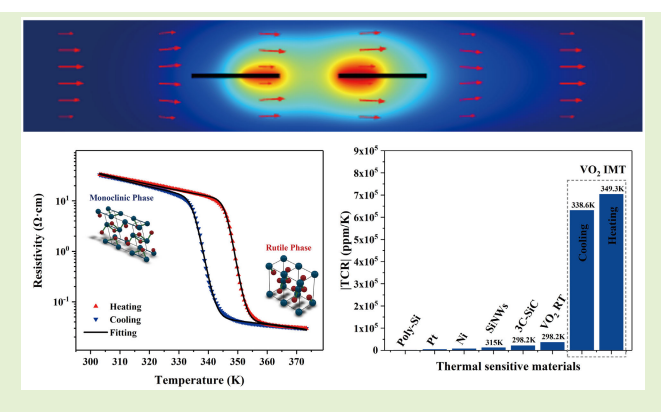


# A Novel Vanadium Dioxide-Based Dual-Heater Microfluidic Thermal Flow Sensor With Record High Sensitivity

Yunqi Cao<sup>®</sup>, *Member, IEEE*, Yushan Zhou<sup>®</sup>, *Student Member, IEEE*, Shuyu Fan<sup>®</sup>, *Student Member, IEEE*, Haozhen Chi<sup>®</sup>, *Student Member, IEEE*, Nelson Sepúlveda<sup>®</sup>, *Senior Member, IEEE*, Dibo Hou<sup>®</sup>, and Hongjian Zhang

Abstract—High-sensitivity flow measurement technology is a prerequisite for precise dynamic control of microfluidics. Despite the advances in structure optimization, a more efficient approach to improve device sensitivity can be realized by leveraging materials with a higher temperature coefficient of resistance (TCR). This work presents the design and simulation of a vanadium dioxide (VO<sub>2</sub>)-based microfluidic thermal flow sensor with record high sensitivity. Owing to the phase change property, VO<sub>2</sub> demonstrates the maximum TCR of -0.703 and -0.63 K<sup>-1</sup> in the major heating and cooling curves, respectively, which is more than two orders of magnitude higher than commonly used thermal-sensitive materials. To fully utilize the high thermal sensitivity of VO<sub>2</sub>, a dual-heater configuration with enhanced thermal differential effect is proposed, and its sensing performance is evaluated in the



flow range below 10  $\mu$ L  $\cdot$  min<sup>-1</sup>. By individually operating the VO<sub>2</sub> thermal sensors at critical transition temperatures in the major hysteresis loop, the sensitivity can reach as high as 2.79 V/ $\mu$ L  $\cdot$  min<sup>-1</sup>, which is about 187.88 times and 277.89 times higher than the VO<sub>2</sub>-based anemometer and the Pt-based dual-heater calorimetric (DHC) sensor, respectively. The research in the present work may enable a breakthrough in the improvement of high-performance microfluidic thermal flow sensors in the ultralow flow region using nonstandard metamaterials.

Index Terms—Dual-heater, microfluidics, phase-change materials (PCMs), thermal flow sensor, vanadium dioxide  $(VO_2)$ .

# I. INTRODUCTION

ICROELECTROMECHANICAL systems (MEMS) have amply demonstrated the ability of microfluidic devices to fully incorporate analytical procedures into flow systems with  $\mu L$  and sub- $\mu L$  volumes [1]. By imparting higher-level performances within a chip via integrating

Manuscript received 31 January 2023; revised 26 February 2023; accepted 27 February 2023. Date of publication 8 March 2023; date of current version 14 March 2024. This work was supported in part by the National Natural Science Foundation of China under Grant 62103369. The associate editor coordinating the review of this article and approving it for publication was Prof. Jeong Bong Lee. (Corresponding author: Yungi Cao.)

Yunqi Cao, Yushan Zhou, Shuyu Fan, Haozhen Chi, Dibo Hou, and Hongjian Zhang are with the State Key Laboratory of Industrial Control Technology, College of Control Science and Engineering, Zhejiang University, Hangzhou, Zhejiang 310027, China (e-mail: caoyunqi@zju.edu.cn).

Nelson Sepúlveda is with the Department of Electrical and Computer Engineering, Michigan State University, East Lansing, MI 48824 USA (e-mail: sepulve6@msu.edu).

Digital Object Identifier 10.1109/JSEN.2023.3251662

functional materials and fluidic structures, planar microfluidic devices can benefit many research fields, including pharmaceutical analysis [2], microorganism analysis [3], chemical synthesis [4], and so on. Given the need for manipulating fluids at the microscale, it is essential to have precise and reliable quantitative techniques to measure the liquid flow in the range of  $1 \text{ nL} \cdot \text{min}^{-1} - 1 \text{ mL} \cdot \text{min}^{-1}$  [5], [6]. In addition, the rapid development of emerging applications such as emulsion generation [7], flow cytometry [8], and flow mixing [9] in the micrototal analytical systems ( $\mu$ -TAS) further imposes flow metering devices with the requirement of ultrahigh sensitivity in the sub-nL range.

Microfluidic thermal flow sensors have attracted great interest among existing sensing mechanisms due to their high sensitivity, high accuracy, and simple implementation [10], [11]. In addition, the measurement of flow rate and other fluidic properties, that is, viscosity [12], wall shear stress [13], and density [14] can also be realized by examining the amount of heat transferred upon a convective flow in anemometric,

1558-1748 © 2023 IEEE. Personal use is permitted, but republication/redistribution requires IEEE permission. See https://www.ieee.org/publications/rights/index.html for more information.

calorimetric, or time-of-flight sensor configurations [15]. The transduction between temperature variations and readout electric signals often relies on standard thermal-sensitive materials such as Pt and Ni, exhibiting a high-temperature coefficient of resistance (TCR) in the range of 3000–7000 ppm  $\cdot$  K<sup>-1</sup> [16] and compatibility with the microfabrication process.

### A. Review of Sensitivity Enhancement Methods

To improve the sensitivity of thermal flow sensors, it is critical to minimize the conductive heat loss through the supporting structures and channel walls. Numerous strategies have been proposed, including constructing clamped-clamped beam structures suspended in the microchannel [17] or vacuum cavities that can isolate thermal transfer to the substrate [18], [19]. Besides, systematic experimental studies have revealed that the sensitivity can be further improved by optimization of the geometric parameters, including the membrane's aspect ratio [20] and shape [21], [22], or by replacing the substrate with lower thermal conductivity materials [23]. All these approaches focus on maximizing the heat transfer from the sensor to the flow, which significantly increases the sensitivity of the thermal flow sensor. Nevertheless, as the foundation of thermo-resistive effect-based flow sensors, the constant search for materials with a higher absolute value of TCR is considered the ultimate approach to breaking through the performance with ultrahigh sensitivity [24].

Efforts to improve thermo-resistive sensitivity intend to explore nonstandard thermal-sensitive semiconducting materials, which show multiple times higher TCR values than conventional metallic materials. Gao et al. [25] improved both the thermal sensitivity and the electrical stability of the single-walled carbon nanotube (SWCNT) thermistor film by the vacuum thermal annealing and electrical aging technique, showing a high TCR of 8040 ppm  $\cdot$  K<sup>-1</sup> in the range of 293-333 K for fluid shear stress measurement. Dao's research group demonstrated highly thermal-sensitive amorphized silicon nanowires (SiNWs) for thermal-sensing applications, and a high negative TCR was measured from -8000 to -12000 ppm · K<sup>-1</sup> [26]. Moreover, Nguyen's research group introduced cubic silicon carbide (3C-SiC) nano-thin films with high TCR of 20720 ppm  $\cdot$  K<sup>-1</sup> at room temperature (RT) and  $-9287 \text{ ppm} \cdot \text{K}^{-1}$  at 473 K [27], [28], demonstrating a potential application for airflow sensing in harsh environments. As one of the most thermally sensitive smart materials, vanadium dioxide (VO<sub>2</sub>) has been widely implemented in thermal-sensitive applications such as temperature sensing [29], light sensing [30], breath sensing [31], frequency tuning [32], and so on. Recently, we demonstrated the potential use of VO<sub>2</sub> as the temperature-driven phase-change material (PCM) in near-RT thermal airflow measurement. The maximum TCR is determined to be  $-0.43 \text{ K}^{-1}$  in its insulatorto-metal transition (IMT) region and  $-24\,000$  ppm  $\cdot$  K<sup>-1</sup> at RT [33], [34], respectively. Although the maximum TCR shows more than 60 times higher than that of Pt, the on-substrate hot-film sensor structure only exhibits a mediocre sensitivity. Therefore, a designated novel sensor configuration is imperative to develop the VO<sub>2</sub>-based thermal flow sensor with ultrahigh flow measurement sensitivity.

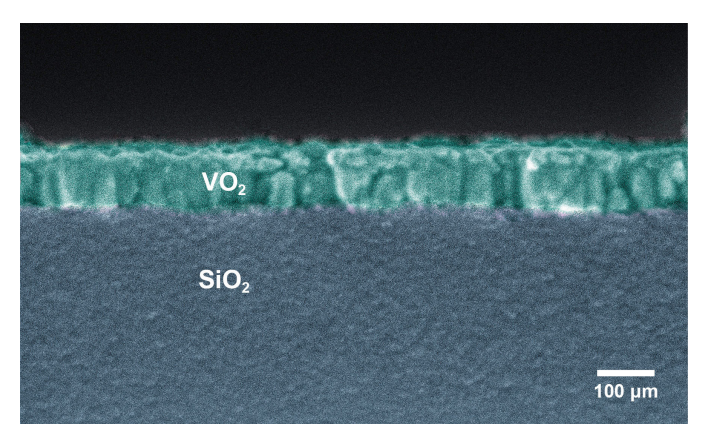


Fig. 1. SEM image of the cross-sectional view of the  $VO_2$  thin film deposited on a  $SiO_2/Si$  substrate.

## B. Contribution of This Work

This work proposes a VO<sub>2</sub>-based microfluidic sensor with a novel dual-heater calorimetric (DHC) sensing configuration to demonstrate the high-sensitivity thermal flow measurement in the ultralow flow range. The VO2 thin film was successfully fabricated by the pulsed laser deposition (PLD) method. The temperature-dependent resistivity was obtained using the four-point probe method with accurately controlled substrate temperature. The resistivity shows a fully reversible hysteretic three-order change in magnitude during the complete heating and cooling cycles. An analytical model was also used to determine the temperature-dependent TCR across the IMT region, where the maximum TCR at the critical transition temperature demonstrates an ultrahigh TCR of -0.703 and  $-0.63 \text{ K}^{-1}$  in the major heating and cooling curves, respectively. To investigate the sensing performance of the DHC sensor, a finite-element analysis (FEA) was carried out to evaluate the heat-transfer process, and the sensing mechanism compared with classical anemometric and calorimetric sensors. The significantly higher sensitivity demonstrated by the VO<sub>2</sub>-based DHC sensor can be attributed to an enhanced thermal differential effect which is also observed in the Pt-based DHC sensor. The research presented in this work provides an effective strategy for implementing nonstandard PCM in developing high-performance microfluidic thermal flow sensors, paving the way toward using high-precision portable analytical instruments and lab-on-a-chip (LOC) devices for cell culture [35], pharmaceutical [36], [37] and point-of-care diagnostic [38] applications.

# II. MATERIALS AND CHARACTERIZATIONS A. Synthesis of VO<sub>2</sub> Thin Film

The temperature-dependent electrical properties of  $VO_2$  are obtained from a  $VO_2$  thin film deposited on a  $SiO_2/Si$  substrate using the PLD method, where the 1- $\mu$ m  $SiO_2$  layer is prepared by plasma-enhanced chemical vapor deposition (PECVD). Fig. 1 shows a cross-sectional scanning electron microscopy (SEM) view image of the fabricated  $VO_2$  thin film of approximately 120-nm thick. During the  $VO_2$  deposition, a turbomolecular pump was connected with a mechanical scroll pump to pump down the process chamber to the vacuum level below

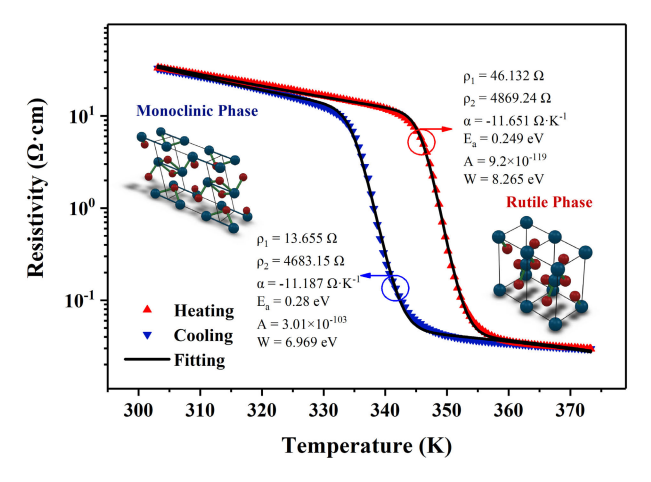


Fig. 2. Resistivity of the VO<sub>2</sub> thin film as a function of temperature during the fully reversible heating and cooling loops, where the fitting parameters and the schematics of the microcrystalline structures are also presented.

0.01 mtorr. Next, oxygen gas was introduced into the chamber at a flow rate of 20 sccm, and the oxygen atmosphere pressure was maintained at 15 mtorr. Then, the 2 inch substrate wafer was radiatively heated by a ceramic heater from the backside at a distance of 1 in. When the temperature reached 868 K, a vanadium target placed 1.75 inches in front of the wafer was ablated by the krypton fluoride (KrF) excimer laser pulses with 352-mJ energy and a repetition rate of 10 Hz for 20 min. After the deposition, the VO<sub>2</sub> thin film was annealed under the same deposition condition for 30 min to allow the growth of VO<sub>2</sub> microcrystalline [39].

### B. Determine VO<sub>2</sub> Resistivity

The resistivity of the VO<sub>2</sub> thin film is measured by the four-point probe method and can be expressed as  $\rho$  =  $4.532tR_s$  [40], where t is the thickness of the VO<sub>2</sub> film and  $R_s$  is the resistance determined by the voltage (V)measured between the inner two probes divided by the current (I) measured between the outer two probes. To study the thermal-electrical resistivity of  $VO_2$ ,  $\rho$  is measured as a function of temperature (T) during the complete heating and cooling cycles between 300 and 374 K. Since the resistivity of VO2 is ultrasensitive to temperature fluctuations, precise control of the substrate temperature is required. This is achieved using a closed-loop controlled temperature control system described in our previous works [33], [41], [42]. Fig. 2 shows the fully reversible hysteretic change in resistivity across the complete major heating and cooling cycles. The temperature-dependent resistivity  $\rho(T)$  exhibits a sharp change at around 344 K, and a nearly 3-order change in magnitude can be observed between the low-temperature monoclinic phase and the high-temperature rutile phase in a small temperature window of about 15 K.

During the IMT region, VO<sub>2</sub> can be considered in the state with the coexistence of both monoclinic and rutile phases [43]. Therefore,  $\rho(T)$  can be modeled by a parallel circuit model [44], which includes two branches of monoclinic-phase resistivity ( $\rho_{\rm m}$ ) and rutile-phase resistivity ( $\rho_{\rm r}$ ) and can be

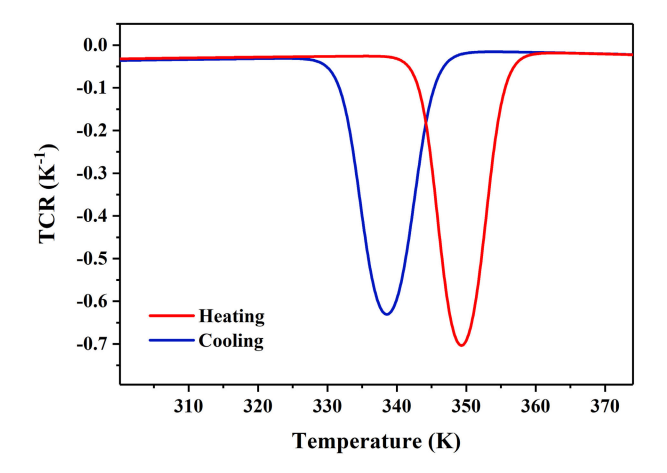


Fig. 3. Temperature-dependent TCR value of  ${\rm VO_2}$  in the major heating and cooling curves across the IMT region.

described as

$$\rho(T) = 4.532t \frac{R_{\rm r}(T)R_{\rm m}(T)}{f_{\rm r}R_{\rm m}(T) + (1 - f_{\rm r})R_{\rm r}(T)}.$$
 (1)

 $R_{\rm m}(T)$ In above equation, the general thermal-activation behavior  $R_{\rm m}(T)$  $4.532t \rho_1 \exp(E_a/k_B T)$  below the IMT region, and  $R_r(T)$ follows the linear temperature dependence in the conducting monoclinic phase as  $R_r(T) = 4.532t(\alpha T + \rho_2)$ . Here,  $E_a$ and  $k_{\rm B}$  are activation energy and Boltzmann's constant, respectively, and  $\alpha$ ,  $\rho_1$ , and  $\rho_2$  are constants. The volume fraction  $f_r$ , which represents the percentage of the monoclinic phase in the phase coexistence state, can be empirically expressed as [44]

$$f_{\rm r}(T) = \frac{1}{1 + A \exp\left(\frac{W}{k_{\rm B}T}\right)} \tag{2}$$

where A is the fitting constant, and W is the transition related energy. Thus,  $\rho(T)$  can be analytically modeled by combining (1) and (2) as presented in Fig. 2.

#### C. Temperature-Dependent TCR

Given the function of  $\rho(T)$ , the temperature-dependent TCR of VO<sub>2</sub>  $[\alpha_v(T)]$  can be calculated as  $\alpha_v(T) =$  $\rho(T)[d\rho(T)/dT]$  across the complete heating and cooling cycles as a function of temperature. As seen in Fig. 3, the maximum values of TCR in the heating and cooling curves appear at different temperatures due to the inherent hysteretic behavior, where the difference in temperature between the two extreme points indicates the width of the IMT region. At transition temperatures defined by the maximum value of TCR,  $\alpha_{\rm v}(T)$  is calculated to be  $-0.703~{\rm K}^{-1}$  at 349.3 K and  $-0.63 \text{ K}^{-1}$  at 338.6 K in the heating and cooling curves, respectively. Note that the TCR values obtained in this work are different from our previous work [34] because distinct VO<sub>2</sub> disposition conditions and substrates are used, which results in a change of microcrystalline structures [39] and electrical properties [45]. However, this work is not focused on the optimization of the VO<sub>2</sub> properties but on trying to establish a sensing mechanism for using the IMT-induced

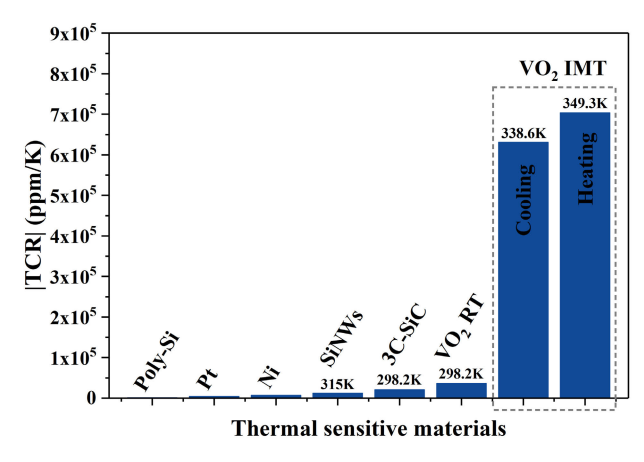


Fig. 4. Comparison of TCR values of VO<sub>2</sub> in different temperature regions with other thermal-sensitive materials.

high thermal sensitivity of VO<sub>2</sub> in microfluidic thermal flowsensing applications.

As shown in Fig. 4, the maximum  $\alpha_v(T)$  in the heating and cooling curves during the IMT region shows nearly two orders of magnitude higher than that of conventional thermal-sensitive materials such as Pt, Ni, and polysilicon (Poly-Si), demonstrating great potential in developing high-sensitive microfluidic thermal flow sensors. Although  $\alpha_{\rm v}(T)$  can only be maintained at the ultrahigh levels in a small temperature window and sharply decreases as the temperature deviates from the critical transition temperatures, it is worth noting that  $\alpha_v(T)$  at RT still exhibits a high value of about  $-36\,100$  ppm  $\cdot$  K<sup>-1</sup>, which is approximately 1.74-3.01 times higher than recently proposed SiNWs and 3C-SiC and 9.21 times higher than the most commonly used metallic thermal-sensing material Pt. Nevertheless, this work presents the design and evaluation of VO2-based highsensitivity microfluidic thermal flow sensors using the phasechange-induced ultrahigh  $\alpha_{\rm v}(T)$  around the critical transition temperatures in the IMT region, developing a new sensing configuration that can alleviate the pain of the inherent nonlinear hysteretic behavior.

# III. SENSOR DESIGN AND WORKING PRINCIPLES A. Dual-Heater Calorimetric Sensor

To implement VO<sub>2</sub> as the sensing element in thermal flow sensors, two classical sensing configurations, including anemometric and calorimetric sensors, are often considered. Fig. 5(a) and (b) show the schematic drawings of such VO<sub>2</sub>-based sensors. The anemometric sensor consists of a stacking structure of the heater-sensor pair and measures the flow rate based on the heat loss from the thermistor (VO<sub>2</sub> in this case) upon a convective flow. On the other hand, the calorimetric sensor evaluates the temperature difference between the upstream and downstream sensors to increase both the sensitivity and the dynamic range. This technique has been used mainly in thermal flow-sensing applications with the microliter and nanoliter flow ranges [36], [37], [46]. However, the traditional calorimetric sensing configuration consists of only one heater. Therefore, the upstream sensor T<sub>a</sub> and the downstream sensor T<sub>b</sub> must share the same

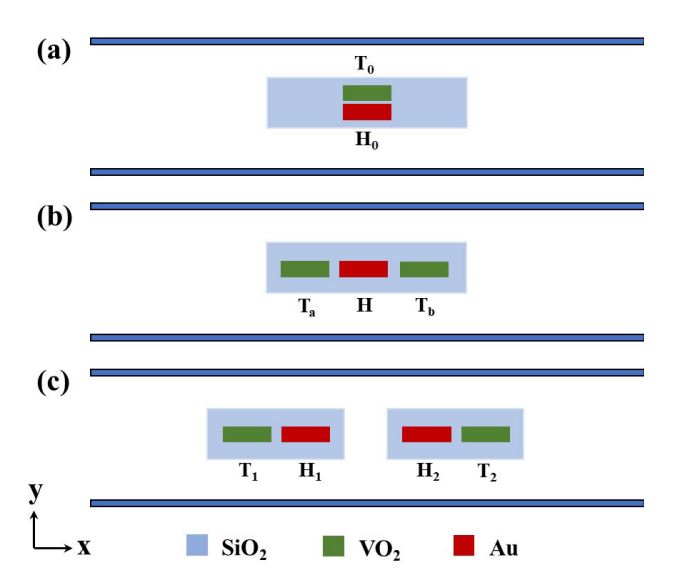


Fig. 5. Comparison of different thermal flow sensor configurations. (a) Anemometric sensor with heater  $H_0$  and sensor  $T_0$  stacking at the same location. (b) Calorimetric sensor with heater H, upstream sensor  $T_a$ , and downstream sensor  $T_b$ . (c) DHC sensor with upstream and downstream heater—sensor pairs  $(T_1, H_1)$  and  $(T_2, H_2)$ .

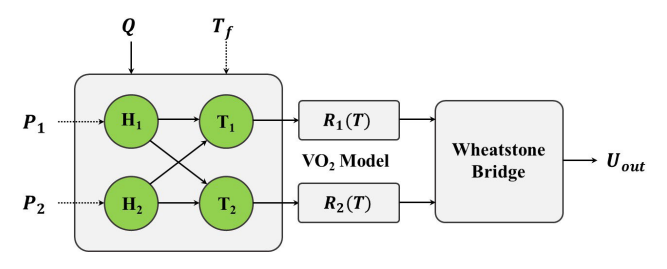


Fig. 6. Illustration of the heat-transfer model for the proposed DHC sensor in the CP mode.

operating temperature when no convective flow is applied in the microchannel. Thus, when  $VO_2$  is used for both  $T_a$  and  $T_b$ , only one  $VO_2$  sensor can be operated following the major hysteresis curve, leaving the other sensor forced into the minor loop with lower thermal sensitivity [33]. To maximize the thermal sensitivity, a new sensor configuration is proposed and schematically shown in Fig. 5(c). Thus, both  $T_1$  and  $T_2$  can be operated individually by heaters  $H_1$  and  $H_2$ , allowing both sensors to work either in the major cooling or heating curve with optimum thermal sensitivity.

### B. Heat Transfer in Dual-Heater Configuration

To better understand the sensing mechanism in the dual-heater configuration, a model illustrating the thermal interaction among heating and sensing elements is presented in Fig. 6 to analyze the heat-transfer process. For each sensor pair, the influence of the heater  $(H_1 \text{ or } H_2)$  on the adjacent sensor  $(T_1 \text{ or } T_2)$  can be analogous to the principle of the calorimetric sensor, as shown in Fig. 5(b), with only the left or right half being considered. Thus, when a small convective flow is applied in the microchannel, the heat flow can cause a temperature decrease in  $H_1$  and an increase in  $H_2$  before the saturation point [47], which follows a similar behavior as that of the calorimeter. However, it can be seen that a

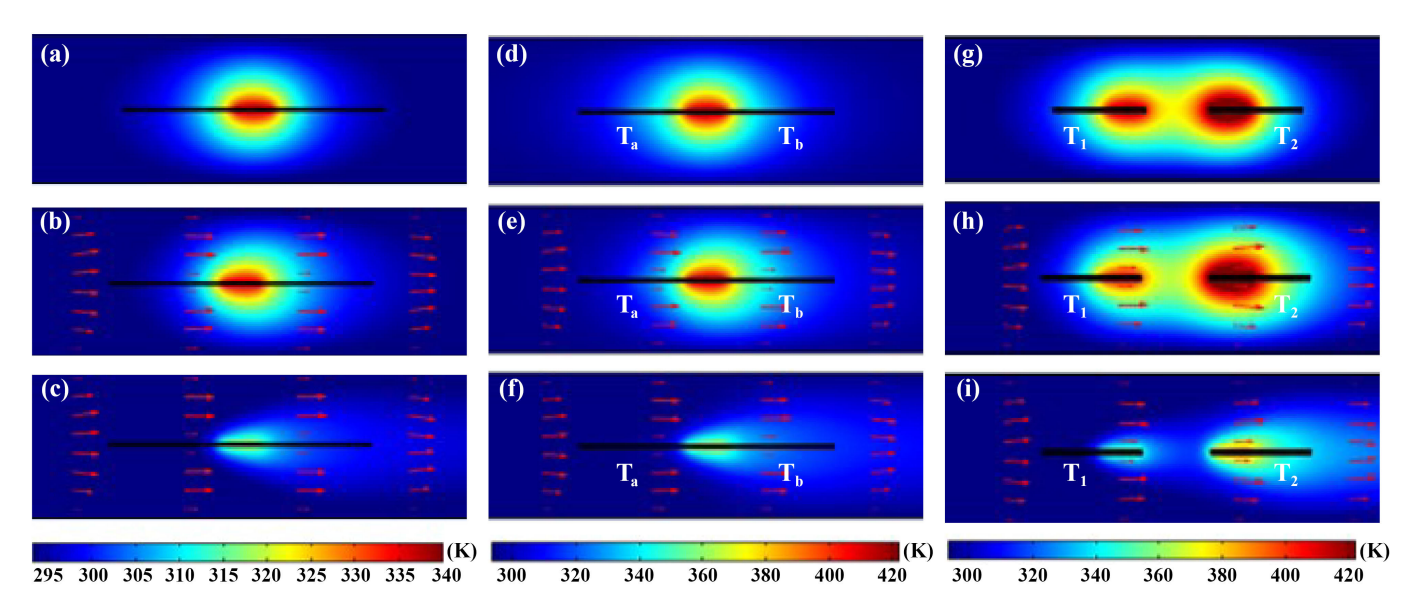


Fig. 7. 2-D FEA results of VO<sub>2</sub>-based microfluidic flow sensors with different sensor configurations. Temperature distribution of a VO<sub>2</sub>-based anemometric sensor under (a) zero-flow, (b) 1  $\mu$ L · min<sup>-1</sup>, and (c) 10  $\mu$ L · min<sup>-1</sup>. Temperature distribution of a VO<sub>2</sub>-based calorimetric sensor under (d) zero-flow, (e) 1  $\mu$ L · min<sup>-1</sup>, and (f) 10  $\mu$ L · min<sup>-1</sup>. Temperature distribution of a VO<sub>2</sub>-based DHC sensor under (g) zero-flow, (h) 1  $\mu$ L · min<sup>-1</sup>, and (i) 10  $\mu$ L · min<sup>-1</sup>. The red arrows represent the direction of forced convective flow in the microchannel.

cross-interaction also exists between  $H_1$  ( $H_2$ ) and  $T_2$  ( $T_1$ ) since the convective flow carries an extra amount of heat to  $T_2$  from  $H_1$  while the influence of  $H_2$  on  $T_1$  is on the opposite due to the symmetric design of the sensor configuration. In short, this preliminary heat analysis reveals that the proposed dual-heater sensor configuration is based on the calorimetric-sensing mechanism with an enhanced differential effect between  $T_1$  and  $T_2$  due to the upstream and downstream cross-interaction.

Two operation modes are often considered for thermal flow sensors, namely, the constant power (CP) mode [48] and the constant temperature (CT) mode [49]. Although the CT mode responds faster to flow rate changes, the requirement of using an ambient-temperature diode or an additional chip significantly increases the manufacturing cost and the operation complexity [49], [50]. Nevertheless, since the primary purpose of this work is to demonstrate high-sensitivity microfluidic thermal flow sensing using VO2, the CP mode is used for simplicity and adequately to prove the concept. For the CP mode shown in Fig. 6, the input power  $P_1$  and  $P_2$  supplied to  $H_1$  and  $H_2$ , respectively, the ambient temperature  $T_f$ , are set to be constant values, while the variable input convective flow rate (Q) alters the temperature distribution between  $T_1$  and T<sub>2</sub>. According to the VO<sub>2</sub> resistance model described before, the sensor resistance  $R_1(T)$  and  $R_2(T)$  can be calculated and converted to an output voltage  $U_{\text{out}}$  through a Wheatstone bridge, thus establishing a relation between  $U_{\text{out}}$  and Q for examining the sensing performance.

# IV. RESULTS AND DISCUSSION A. 2-D FEA Simulation

To fully investigate the sensing performance of the proposed VO<sub>2</sub>-based DHC sensor compared with other sensing mechanisms, a 2-D FEA is carried out using COMSOL Multiphysics to evaluate the heat-transfer properties in a deionized water

(DI) environment shown in Fig. 7. The microchannel in the simulation has a length of 600  $\mu$ m and a height of 80  $\mu$ m. The materials used for the upper and lower channel substrates are polydimethylsiloxane (PDMS) and Si, respectively. To minimize stray heat loss through conduction heat transfer, all sensing and heating elements shown in Fig. 5 are encapsulated in the middle of suspended SiO<sub>2</sub> clamped-clamped microbridges with the same thickness of 2  $\mu$ m. The width of the Au microbridge is 140  $\mu$ m for the calorimetric sensor and 52  $\mu$ m for both upstream and downstream microbridges in the dualheater configuration. In addition, the distances between the heater and the sensor in Fig. 5(b) and (c), and the upstream and downstream heater-sensor pairs are set to be 10 and 36  $\mu$ m, respectively. It should be noted that the anemometric sensor shown in Fig. 5(a) has the sensor and the heater stacked at the same location, which is different from the calorimetric sensor and the DHC sensor. Thus, an insulation layer of 200-nm SiO<sub>2</sub> is applied between T<sub>0</sub> and H<sub>0</sub> to avoid the short-circuit fault in the actual device fabrication.

Fig. 7(a) shows the temperature distribution of a VO<sub>2</sub>-based anemometric sensor under the zero-flow condition. Since the temperature decreases with the flow rate, the initial temperature of the sensor is 338.6 K in the major cooling curve, which corresponds to a constant heater power of 21.26 mW. The flow rates increase to 1 and 10  $\mu$ L  $\cdot$  min<sup>-1</sup> shown in Fig. 7(b) and (c), respectively. The temperature decreases due to the convection loss while a thermal boundary layer is formed in the vicinity of the microbridge. Differently, the calorimetric sensor only consists of one heating element, meaning both Ta and Tb can only be set at the same initial temperature of either 338.6 K in the major cooling curve (62.56 mW) or 349.6 K in the major heating curve (78.06 mW). Fig. 7(d)–(f) shows the temperature distribution of a calorimetric sensor under different flow rates with an initial temperature of 338.6 K in the major cooling curve.

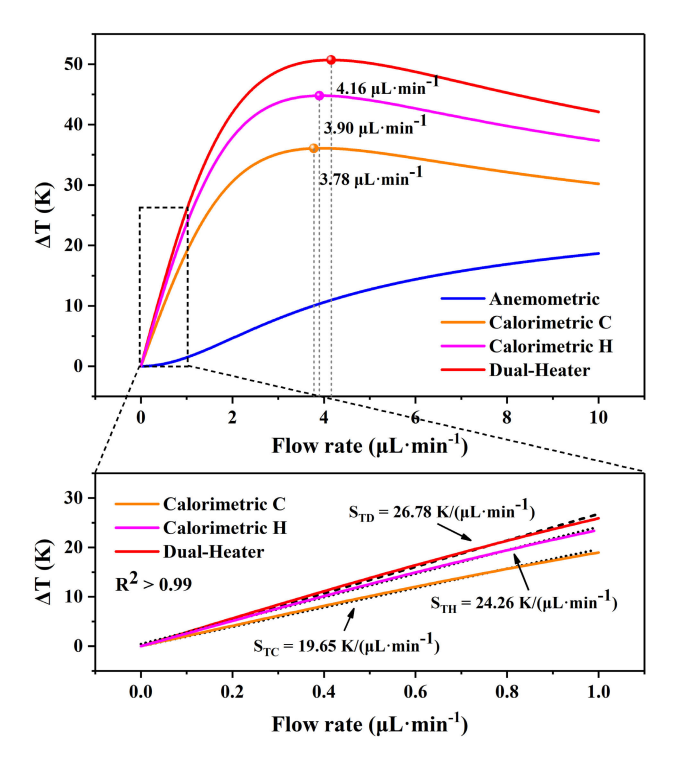


Fig. 8. Simulation results of the temperature change in VO<sub>2</sub> sensors with different sensing configurations under forced convection flow in the range of 0–10  $\mu$ L  $\cdot$  min<sup>-1</sup>. The magnified region shows the linear response range of the calorimetric and dual-heater sensors.

Although the temperature difference ( $\Delta T$ ) between  $T_a$  and  $T_b$ can be utilized to determine the flow rate, especially in the low flow rate range, this configuration is not ideal for VO<sub>2</sub>-based thermal flow sensors discussed in Section III. Nevertheless, the VO<sub>2</sub>-based calorimetric sensor is a comparison to demonstrate the enhanced thermal differential effect of the proposed DHC sensor. The dual-heater configuration allows individual temperature control of T<sub>1</sub> and T<sub>2</sub> through H<sub>1</sub> and H<sub>2</sub>, respectively. Therefore, it is physically allowed to have  $T_1$  and  $T_2$  both working with the optimum TCRs. In this case, the initial temperatures of T<sub>1</sub> and T<sub>2</sub> are 338.6 and 349.6 K in the major cooling and heating curves, respectively. As shown in Fig. 7(g)–(i), the convection flow causes a higher temperature in the downstream heater-sensor pair. By comparing Fig. 7(f) and (i), it can be seen that this  $\Delta T$  in  $T_1$  and  $T_2$  is more significant than that in Ta and Tb, demonstrating an enhanced thermal differential effect in the DHC sensor.

### B. Performance of VO<sub>2</sub>-Based Thermal Flow Sensors

Fig. 8 shows the simulation results of  $\Delta T$  in VO<sub>2</sub> sensors with three different sensing configurations in the flow range of 0–10  $\mu$ L · min<sup>-1</sup>, where  $\Delta T$  is defined as  $T_0-T_f$  for the anemometric sensor and the temperature difference between the downstream and upstream sensors for others. Since the calorimetric sensor can only have one sensor operating with the optimum thermal sensitivity, two operating modes are considered, namely calorimetric C and calorimetric H, which corresponds to 338.6 and 349.6 K in the major cooling and heating curves, respectively. It can be seen in Fig. 8 that both

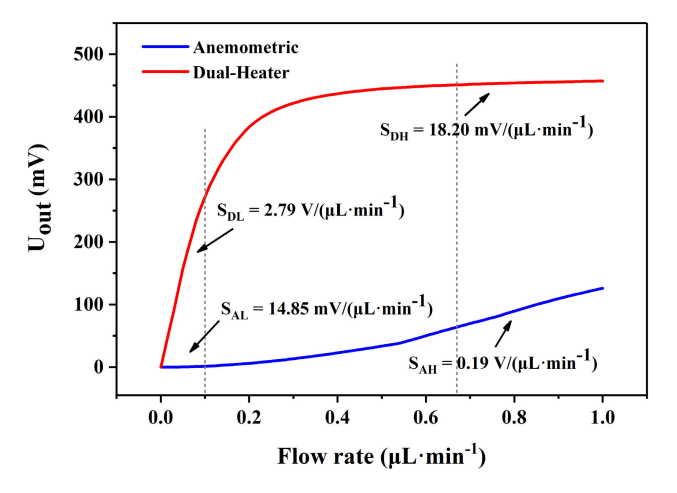


Fig. 9. Simulation results of  $U_{\rm out}$  at the Wheatstone bridge for VO<sub>2</sub>-based microfluidic thermal flow sensors with anemometric and dual-heater configurations operating at optimal working conditions.

types of calorimetric sensors and the DHC sensor show higher thermal sensitivity than the anemometric sensor in the lower flow range due to the thermal differential effect. However, as the flow rate further increases, the temperature in the downstream sensor starts to decrease due to the convection heat loss, leading to a lower  $\Delta T$ . Thus, a saturation turning point of 3.78, 3.90, and 4.16  $\mu$ L · min<sup>-1</sup> can be observed for calorimetric C, calorimetric H, and dual-heater sensors, respectively. Since the type H calorimetric sensor is operated at a higher initial temperature and requires more mass flow to dissipate heat, its turning point occurs at a slightly larger flow rate than the calorimetric C sensor. As for the DHC sensor, the turning point is higher than both calorimetric sensors, indicating a greater monotonic range used for flow rate measurement. This can be attributed to the implementation of an additional heater, which carries more heat to the downstream sensor and thus defers the turning point to a higher flow rate. In addition, the sensing performance is also investigated in the linear range defined as  $R^2 > 0.99$ . It can be seen in Fig. 8 that the DHC sensor shows a high-sensitivity  $S_{TD}$  of 26.78 K/( $\mu$ L·min<sup>-1</sup>), which is 10.39% and 36.28% higher than  $S_{TH}$  and  $S_{TC}$  of type H and C calorimetric sensors, respectively. Therefore, the enhanced thermal differential effect is demonstrated.

The output voltages  $(U_{out})$  of different VO<sub>2</sub>-based sensors at the Wheatstone bridge are simulated in the range of  $0-1 \mu L \cdot min^{-1}$  and shown in Fig. 9. It is worth mentioning that the comparison with the calorimetric sensor is not included in this discussion because this configuration is not ideal for VO2-based thermal flow sensors as demonstrated in previous sections. Although  $\Delta T$  shows a linear response to the flow rate in this range,  $U_{\text{out}}$  shows a different behavior according to the nonlinear hysteretic model of VO<sub>2</sub>. In this case, the DHC sensor exhibits a linear response in the flow range of 0–0.1  $\mu$ L · min<sup>-1</sup>. The sensitivity  $S_{DL}$  in this range is determined to be 2.79 V/( $\mu$ L · min<sup>-1</sup>), which is around 188 times higher than the anemometric sensor with  $S_{AL}$  of 14.85 mV/( $\mu$ L · min<sup>-1</sup>) in the same flow range. When the flow rate is further increased,  $\Delta T$  becomes greater than the hysteresis width, which results in a sharp decrease

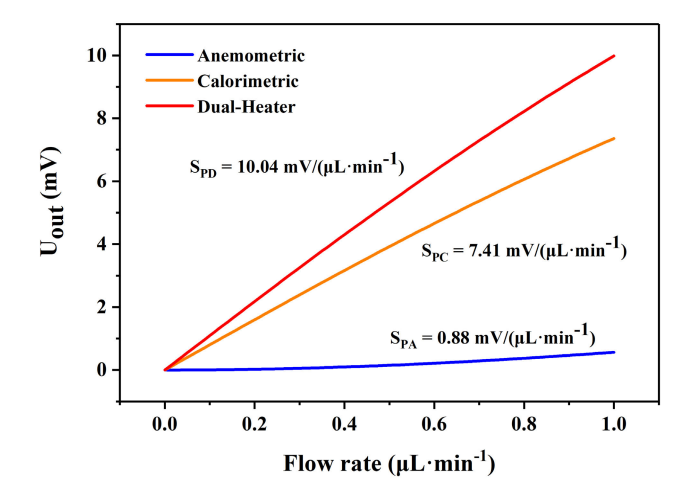


Fig. 10. Simulation results of  $U_{\rm out}$  at the Wheatstone bridge for Pt-based microfluidic thermal flow sensors with three different sensing configurations.

in the TCR. Thus, the sensitivity starts to decrease, and a turning point occurs at a lower flow rate than that shown in Fig. 8. However, in the higher linear flow range from 0.67 to  $1 \mu L \cdot min^{-1}$ , the sensitivity  $S_{AH}$  of the anemometric sensor is much higher than  $S_{DH}$ . Thus, the DHC sensor is more suitable for ultralow flow rate measurement in the nL range.

To further demonstrate the sensitivity of the VO<sub>2</sub>-based DHC sensor and the enhanced thermal differential effect, simulations on Pt-based flow sensors are also performed with the same configuration, that is, the same structure and geometric parameters. Since the Pt has a constant TCR value, the initial temperatures for all VO<sub>2</sub> sensors are set at 338.6 K. As shown in Fig. 10,  $U_{\text{out}}$  exhibits a linear response for all sensing configurations in the flow range of 0–1  $\mu$ L · min<sup>-1</sup>. It can also be found that the Pt-based DHC sensor shows a higher sensitivity than the other two configurations, indicating the enhanced thermal differential effect does not require the downstream sensor T<sub>2</sub> to have a higher temperature. In short, the cross-interaction between sensor pairs is the key to increasing  $\Delta T$  and sensitivity. In comparison with Fig. 9, it can be seen that the VO<sub>2</sub>-based DHC sensor has a sensitivity of 1.81 to 277.89 times higher than the Pt-based DHC sensor.

#### V. CONCLUSION

This article proposes a novel  $VO_2$ -based microfluidic thermal flow sensor with a dual-heater configuration for ultrahigh sensitivity measurement of flow rate in the nanoliter region. The high thermal sensitivity of  $VO_2$  thin film is verified by the resistivity measurement throughout the complete heating and cooling cycles, which shows a fully reversible hysteretic 3-order change in the resistivity. An analytical model has also been used to predict the resistivity change as a function of temperature accurately. Therefore, the maximum TCR values are determined to be 0.703 and 0.63  $K^{-1}$  at transition temperatures in the heating and cooling curves. A dual-heater configuration is designed to maximize the sensing performance, which

allows both upstream and downstream  $VO_2$  sensors to be operated at their optimum working temperatures. In addition, the implementation of the extra heater induces an enhanced thermal differential effect which magnifies the temperature difference between the two  $VO_2$  sensors. Results show that the thermal sensitivity of the DHC can be 36.28% higher than the classical calorimetric sensor in the flow range of 0–0.1  $\mu$ L · min<sup>-1</sup>. Compared to the anemometric sensor, the DHC sensor demonstrates an ultrahigh device sensitivity of 2.79  $V/(\mu$ L · min<sup>-1</sup>) in the range of 0–0.1  $\mu$ L · min<sup>-1</sup>, which is more than 187 times and 277 times higher than that of the  $VO_2$ -based anemometer and the Pt-based DHC sensor.

It is worth mentioning that although the proposed sensor configuration shows a promising sensing mechanism in ultrahigh sensitivity thermal flow rate measurement, more considerations need to be included in future work for both performance optimization and device realization. For instance, the distance between upstream and downstream heater-sensor pairs is an essential geometric parameter that affects the sensing performance, because the cross-interaction between  $H_1$  ( $H_2$ ) and  $T_2$  ( $T_1$ ) depends on the amount of heat transfer as a function of distance. In addition, the CT mode also needs to be considered and compared with the CP mode for a thorough performance evaluation. It should also be noted that hysteretic behavior can still bring some limitations in practice even if the DHC sensor is used. This is because the fluctuations in the flow rate can cause a significant thermal variation and thus force the sensor into a minor hysteresis loop, resulting in an incorrect measurement due to accumulated temperature deviations. Therefore, a micro Tesla valve may eliminate the flow fluctuations by restricting the reverse flow in the microchannel. Besides, a proportional-integral-derivative (PID) controller is also indispensable to accurately maintain the VO2 sensors at desired temperatures for the DHC sensor to be operated in the CT mode. Nevertheless, the proposed sensing mechanism may pave the way toward using PCM with ultrahigh thermal sensitivity for microfluidic flow measurement in nL and sub-nL ranges.

### **ACKNOWLEDGMENT**

The authors would like to thank Dr. Rafmag Cabrera and Dr. Tongyu Wang for their insightful discussions.

#### REFERENCES

- E. Verpoorte and N. F. De Rooij, "Microfluidics meets MEMS," Proc. IEEE, vol. 91, no. 6, pp. 930–953, Jun. 2003.
- [2] P. Cui and S. Wang, "Application of microfluidic chip technology in pharmaceutical analysis: A review," J. Pharmaceutical Anal., vol. 9, no. 4, pp. 238–247, Aug. 2019.
- [3] W. Zhou, J. Le, Y. Chen, Y. Cai, Z. Hong, and Y. Chai, "Recent advances in microfluidic devices for bacteria and fungus research," *TrAC Trends Anal. Chem.*, vol. 112, pp. 175–195, Mar. 2019.
- [4] K. S. Elvira, X. C. I. Solvas, R. C. R. Wootton, and A. J. deMello, "The past, present and potential for microfluidic reactor technology in chemical synthesis," *Nature Chem.*, vol. 5, no. 11, pp. 905–915, Oct. 2013.
- [5] C. Cavaniol, W. Cesar, S. Descroix, and J.-L. Viovy, "Flowmetering for microfluidics," *Lab a Chip*, vol. 22, no. 19, pp. 3603–3617, Sep. 2022.
- [6] Z. Fang et al., "Digital microfluidic meter-on-chip," Lab a Chip, vol. 20, no. 4, pp. 722–733, Dec. 2020.

- [7] A. S. Utada, E. Lorenceau, D. R. Link, P. D. Kaplan, H. A. Stone, and D. A. Weitz, "Monodisperse double emulsions generated from a microcapillary device," *Science*, vol. 308, no. 5721, pp. 537–541, Apr. 2005.
- [8] B. Patra, C.-C. Peng, W.-H. Liao, C.-H. Lee, and Y.-C. Tung, "Drug testing and flow cytometry analysis on a large number of uniform sized tumor spheroids using a microfluidic device," *Sci. Rep.*, vol. 6, no. 1, pp. 1–12, Feb. 2016.
- [9] H. A. Stone, A. D. Stroock, and A. Ajdari, "Engineering flows in small devices: Microfluidics toward a lab-on-a-chip," *Annu. Rev. Fluid Mech.*, vol. 36, pp. 381–411, Jan. 2004.
- [10] W. Xu, X. Wang, X. Zhao, and Y.-K. Lee, "Two-dimensional CMOS MEMS thermal flow sensor with high sensitivity and improved accuracy," *J. Microelectromech. Syst.*, vol. 29, no. 2, pp. 248–254, Apr. 2020.
- [11] A. Talbi et al., "A micro-scale hot wire anemometer based on low stress (Ni/W) multi-layers deposited on nano-crystalline diamond for air flow sensing," *J. Micromech. Microeng.*, vol. 25, no. 12, Nov. 2015, Art. no. 125029.
- [12] I. Etchart et al., "MEMS sensors for density-viscosity sensing in a low-flow microfluidic environment," Sens. Actuators A, Phys., vol. 141, no. 2, pp. 266–275, Feb. 2008.
- [13] C. Ghouila-Houri et al., "High temperature gradient calorimetric wall shear stress micro-sensor for flow separation detection," *Sens. Actuators A, Phys.*, vol. 266, no. 15, pp. 232–241, Oct. 2017.
- [14] M. Gonzalez, H. R. Seren, G. Ham, E. Buzi, G. Bernero, and M. Deffenbaugh, "Viscosity and density measurements using mechanical oscillators in oil and gas applications," *IEEE Trans. Instrum. Meas.*, vol. 67, no. 4, pp. 804–810, Apr. 2017.
- [15] F. Ejeian et al., "Design and applications of MEMS flow sensors: A review," Sens. Actuators A, Phys., vol. 295, pp. 483–502, Aug. 2019.
- [16] J. T. W. Kuo, L. Yu, and E. Meng, "Micromachined thermal flow sensors—A review," *Micromachines*, vol. 3, no. 3, pp. 550–573, Jul. 2012.
- [17] W. Xu, X. Wang, R. Wang, J. Xu, and Y.-K. Lee, "CMOS MEMS thermal flow sensor with enhanced sensitivity for heating, ventilation, and air conditioning application," *IEEE Trans. Ind. Electron.*, vol. 68, no. 5, pp. 4468–4476, May 2021.
- [18] M. Dijkstra, M. J. de Boer, J. W. Berenschot, T. S. J. Lammerink, R. J. Wiegerink, and M. Elwenspoek, "Miniaturized thermal flow sensor with planar-integrated sensor structures on semicircular surface channels," Sens. Actuators A, Phys., vol. 143, no. 1, pp. 1–6, 2008.
- [19] Y. Ou et al., "A MEMS thermal shear stress sensor produced by a combination of substrate-free structures with anodic bonding technology," Appl. Phys. Lett., vol. 109, no. 2, Jul. 2016, Art. no. 023512.
- [20] Z. Mehmood, I. Haneef, S. Z. Ali, and F. Udrea, "Sensitivity enhancement of silicon-on-insulator CMOS MEMS thermal hot-film flow sensors by minimizing membrane conductive heat losses," *Sensors*, vol. 19, no. 8, p. 1860, Apr. 2019.
- [21] F. Shaun et al., "Sensitivity optimization of micro-machined thermoresistive flow-rate sensors on silicon substrates," *J. Micromech. Micro*eng., vol. 28, no. 7, Apr. 2018, Art. no. 074002.
- [22] C.-H. Wu, D. Kang, P.-H. Chen, and Y.-C. Tai, "MEMS thermal flow sensors," Sens. Actuators A, Phys., vol. 241, pp. 135–144, Apr. 2016.
- [23] F. Shaun, H. Regina, F. Marty, E. Nefzaoui, T. Bourouina, and W. Cesar, "Design of micro-fabricated thermal flow-rate sensor for water network monitoring," in *Proc. Symp. Design, Test, Integr. Packag.* MEMS/MOEMS (DTIP), May 2017, pp. 1–4.
- [24] T. Dinh, H. P. Phan, A. Qamar, P. Woodfield, N. T. Nguyen, and D. V. Dao, "Thermoresistive effect for advanced thermal sensors: Fundamentals, design considerations, and applications," *J. Microelectromech. Syst.*, vol. 26, no. 5, pp. 966–986, Oct. 2017.
- [25] W. Gao, B. Ma, J. Luo, and J. Deng, "High sensitive polyimide-based single-walled carbon nanotube thermal film sensor for fluid shear stress measurements," Smart Mater. Struct., vol. 28, no. 7, 2019, Art. no. 075021.
- [26] T. Dinh et al., "High thermosensitivity of silicon nanowires induced by amorphization," *Mater. Lett.*, vol. 177, no. 15, pp. 80–84, Aug. 2016.
- [27] T. Dinh, H. P. Phan, N. Kashaninejad, T. K. Nguyen, D. V. Dao, and N. T. Nguyen, "An on-chip SiC MEMS device with integrated heating, sensing, and microfluidic cooling systems," *Adv. Mater. Interfaces*, vol. 5, no. 20, Aug. 2018, Art. no. 1800764.

- [28] V. Balakrishnan et al., "A hot-film air flow sensor for elevated temperatures," Rev. Sci. Instrum., vol. 90, no. 1, Jan. 2019, Art. no. 015007.
- [29] K. Liu, S. Lee, S. Yang, O. Delaire, and J. Wu, "Recent progresses on physics and applications of vanadium dioxide," *Mater. Today*, vol. 21, no. 8, pp. 875–896, Oct. 2018.
- [30] S. Kabir et al., "Phase change vanadium dioxide light sensors," Appl. Mater. Today, vol. 21, Dec. 2020, Art. no. 100833.
- [31] T. Chang et al., "Multifunctional flexible vanadium dioxide films," Accounts Mater. Res., vol. 2, no. 9, pp. 714–725, Aug. 2021.
- [32] Z. Chen, Y. Cao, Y. He, and W. Tian, "A thermally activated VO<sub>2</sub>-based attenuator with SRR structure," *Mater. Des.*, vol. 223, Nov. 2022, Art. no. 111260.
- [33] Y. Cao, T. Wang, and N. Sepúlveda, "Microfluidic thermal flow sensor based on phase-change material with ultra-high thermal sensitivity," *J. Mater. Chem. C*, vol. 11, no. 4, pp. 1278–1284, Jan. 2023.
- [34] Y. Zhou, X. Wang, D. Hou, H. Zhang, N. Sepúlveda, and Y. Cao, "Vanadium dioxide-based high sensitivity dual-heater calorimetric microfluidic sensor," in *Proc. IEEE Sensors*, Dec. 2022, pp. 1–4.
- [35] J. Etxebarria, J. Berganzo, J. Elizalde, G. Llamazares, L. J. Fernández, and A. Ezkerra, "Low cost polymeric on-chip flow sensor with nanoliter resolution," *Sens. Actuators B, Chem.*, vol. 235, pp. 188–196, Nov. 2016.
- [36] J. Kim, H. Cho, S.-I. Han, A. Han, and K.-H. Han, "A disposable microfluidic flow sensor with a reusable sensing substrate," *Sens. Actu*ators B, Chem., vol. 288, pp. 147–154, Jun. 2019.
- [37] D. Lee et al., "Sensitive and reliable thermal micro-flow sensor for a drug infusion system," Sens. Actuators A, Phys., vol. 309, Jul. 2020, Art. no. 112033.
- [38] K. Kwon et al., "An on-skin platform for wireless monitoring of flow rate, cumulative loss and temperature of sweat in real time," *Nature Electron.*, vol. 4, no. 4, pp. 302–312, Mar. 2021.
- [39] N. Sepúlveda, A. Rúa, and F. E. Fernández, "Resonant frequency behavior of silicon cantilevers coated with nanostructured and microcrystalline VO<sub>2</sub> films," *IEEE Trans. Nanotechnol.*, vol. 9, no. 3, pp. 330–334, May 2010.
- [40] I. Miccoli, F. Edler, H. Pfnür, and C. Tegenkamp, "The 100th anniversary of the four-point probe technique: The role of probe geometries in isotropic and anisotropic systems," *J. Phys., Condens. Matter*, vol. 27, no. 22, 2015, Art. no. 223201.
- [41] Y. Cao, D. Hernandez-Escobar, C. Boehlert, and N. Sepulveda, "Actuation dependency of frequency tuning in MEMS resonators," J. Microelectromech. Syst., vol. 29, no. 2, pp. 132–134, Apr. 2020.
- [42] Y. Cao and N. Sepúlveda, "Interface stress for bidirectional frequency tuning of prebuckled vanadium dioxide MEMS resonators," Adv. Mater. Interfaces, vol. 6, no. 21, Sep. 2019, Art. no. 1900887.
- [43] Y. C. Chang et al., "Phase coexistence in the metal-insulator transition of a VO<sub>2</sub> thin film," *Thin Solid Films*, vol. 486, nos. 1–2, pp. 46–49, Aug. 2005.
- [44] X. Zhong, X. Zhang, A. Gupta, and P. LeClair, "Avalanche breakdown in microscale VO<sub>2</sub> structures," *J. Appl. Phys.*, vol. 110, no. 8, Oct. 2011, Art. no. 084516.
- [45] R. E. Marvel, R. H. Robert, C. Valentin, R. R. Bridget, and R. F. Haglund Jr., "Influence of deposition process and substrate on the phase transition of vanadium dioxide thin films," *IEEE Trans. Nanotechnol.*, vol. 91, no. 1, pp. 217–334, Mar. 2015.
- [46] Y. Zhu et al., "Proteomic analysis of single mammalian cells enabled by microfluidic nanodroplet sample preparation and ultrasensitive NanoLC-MS," Angew. Chem., vol. 130, no. 1, pp. 12550–12554, May 2018.
- [47] V. Kitsos, A. Demosthenous, and X. Liu, "A smart dual-mode calorimetric flow sensor," *IEEE Sensors J.*, vol. 20, no. 3, pp. 1499–1508, Feb. 2020.
- [48] T. Glatzl et al., "Hot-film and calorimetric thermal air flow sensors realized with printed board technology," J. Sensors Sensor Syst., vol. 5, no. 2, pp. 283–291, Jul. 2016.
- [49] P. Lange, M. Weiss, and S. Warnat, "Characteristics of a micro-mechanical thermal flow sensor based on a two hot wires principle with constant temperature operation in a small channel," *J. Micromech. Microeng.*, vol. 24, no. 12, Nov. 2014, Art. no. 125005.
- [50] K. A. A. Makinwa and J. H. Huijsing, "Constant power operation of a two-dimensional flow sensor," *IEEE Trans. Instrum. Meas.*, vol. 51, no. 4, pp. 840–844, Aug. 2002.



Yunqi Cao (Member, IEEE) received the B.S. degree in physics from Wuhan University, Wuhan, Hubei, China, in 2012, the M.S. degree in materials science and engineering from the University of Florida, Gainesville, FL, USA, in 2014, and the Ph.D. degree in electrical engineering from Michigan State University, East Lansing, MI, USA, in 2019.

He has worked as a Research and Development Engineer with Semiconductor Manufacturing International Corporation, Shanghai, China,

in 2015. He has served as a Postdoctoral Scholar with the University of Southern California, Los Angeles, CA, USA, from 2019 to 2020. He is currently a tenure-track Faculty Member with the College of Control Science and Engineering, Zhejiang University, Hangzhou, Zhejiang, China. His research interests include microelectromechanical systems (MEMS), microfluidic devices, flexible electronics, and energy harvesting.



Yushan Zhou (Student Member, IEEE) received the B.Eng. degree in chemical engineering from the Zhejiang University of Technology, Hangzhou, Zhejiang, China, in 2021. She is currently pursuing the Ph.D. degree in control science and engineering with the College of Control Science and Engineering, Zhejiang University, Hangzhou.

Her current research interests include microfluidics devices, flow measurement and instrumentation, and phase-change materials.



Shuyu Fan (Student Member, IEEE) received the B.Eng. degree in automation from Zhejiang University, Hangzhou, Zhejiang, China, in 2019, where he is currently pursuing the Ph.D. degree in control science and engineering with the College of Control Science and Engineering.

His current research interests include energy harvesting systems, self-powered smart sensors, human health monitoring, and wearable electronics.



Nelson Sepúlveda (Senior Member, IEEE) received the B.S. degree in electrical and computer engineering from the University of Puerto Rico, Mayagüez, Puerto Rico, in 2001, and the M.S. and Ph.D. degrees in electrical and computer engineering from Michigan State University (MSU), East Lansing, MI, USA, in 2002 and 2005, respectively.

During his last year of graduate school, he attended Sandia National Laboratories, Albuquerque, NM, USA. He joined the Depart-

ment of Electrical and Computer Engineering, University of Puerto Rico, as a Faculty Member, in 2006. He was a Visiting Faculty Researcher with Air Force Research Laboratories, Dayton, OH, USA, in 2006, 2007, 2013, and 2014, the National Nanotechnology Infrastructure Network in 2008, and the Cornell Center for Materials Research in 2009, the last two being the National Science Foundation (NSF)-funded centers at Cornell University, Ithaca, NY, USA. In 2011, he has joined as a Faculty Member at the Department of Electrical and Computer Engineering, MSU, where he is currently a Full Professor. His current research interests include smart materials and the integration of such in microelectromechanical systems, with a particular emphasis on vanadium dioxide thin films and the use of the structural phase transition for the development of smart microactuators.

Dr. Sepúlveda has received the NSF CAREER Award in 2010 and the MSU Teacher-Scholar Award in 2015.



**Dibo Hou** received the B.E. degree in industrial automation and the Ph.D. degree in control science and engineering from Zhejiang University, Hangzhou, China, in 1999 and 2004, respectively.

He is a Full Professor and the Deputy Dean of the College of Control Science and Engineering, Zhejiang University. He is also an Affiliate Member with the State Key Laboratory of Industrial Control Technology, Zhejiang University. He is the author or a coauthor of more than

80 articles in refereed journals. His main research interests include smart sensing and measurement, environmental monitoring and early warning, nondestructive testing, and intelligent information processing.

Dr. Hou is a member of the National Technical Committee on Industrial Process Measurement and Control of Standardization Administration of China. He was selected as the "New Century 151 Talent" of Zhejiang Province in 2015.



Haozhen Chi (Student Member, IEEE) received the B.Eng. degree in automation from Zhejiang University, Hangzhou, Zhejiang, China, in 2019, where he is currently pursuing the Ph.D. degree with the College of Control Science and Engineering.

His current research interests include bionic robotics, motion control, smart materials-based soft actuators, flexible tactile sensors, and structural health monitoring.



Hongjian Zhang received the B.E. degree in chemical automation and the M.S. degree in industrial automation from Zhejiang University, Hangzhou, China, in 1982 and 1985, respectively, and the Ph.D. degree in thermal engineering from the Shanghai Institute of Mechanical Engineering, Shanghai, China, in 1988.

He was the Dean of the College of Control Science and Engineering, Zhejiang University, where he is currently a Full Professor. He was

the Vice President of Zhejiang University. His research interests include detection technology and automatic equipment.